EUROPEAN ORGANIZATION FOR NUCLEAR RESEARCH

CERN-EP/87-231
December 23rd, 1987

EXCLUSIVE ρ^0 AND ϕ PRODUCTION IN DEEP INELASTIC MUON SCATTERING

The European Muon Collaboration

Aachen[1], CERN[2], Freiburg[3], Hamburg[4], Heidelberg[5], Lancaster[6], LAPP (Annecy)[7], Liverpool[8], Marseille[9], Mons[10], Oxford[11], Rutherford[12], Sheffield[13], Turin[14], Uppsala[15], Warsaw[16], Wuppertal[17], Yale[18].

J. Ashman[13], B. Badelek[16a)], G. Baum[18b)], J. Beaufays[2], C.P. Bee[8], C. Benchouk[9], I.G. Bird[6c)], S.C. Brown[8d)], M.C. Caputo[18], H.W.K. Cheung[11], J. Chima[12e)], J. Ciborowski[16a)], R.W. Clifft[12], G. Coignet[7], F. Combley[13], G. Court[8], G D'Agostini[9], J. Drees[17], M. Düren[1], N. Dyce[6], A.W. Edwards[17f)], M. Edwards[12], T. Ernst[3], M.I. Ferrero[14], J. Foster[13g)], D. Francis[8], E. Gabathuler[8], J. Gajewski[4], R. Gamet[8], N. Geddes[12h)], V. Gibson[11i)], J. Gillies[11], P. Grafström[15i)], K. Hamacher[17], D.v. Harrach[5], P. Hayman[8], C.A. Heusch[2j)], J.R. Holt[8], V.W. Hughes[18], A. Jacholkowska[2k)], F. Janata[4l)], G. Jancso[2m)], T. Jones[8], E.M. Kabuss[3c)], B. Korzen[17], U. Krüner[17], S. Kullander[15], U. Landgraf[3], D. Lanske[1], F. Lettenström[15], T. Lindqvist[15], J. Loken[11], M. Matthews[8], Y. Mizuno[5], K. Mönig[17], F. Montanet[9i)], J. Nassalski[16n)], E. Nagy[7m)], P.R. Norton[12], G. Oakham[12o)], R. Oppenheim[18p)], A.M. Osborne[2], V. Papavassiliou[18], N. Pavel[17], C. Peroni[14], H. Peschel[17], R. Piegaia[18], B. Pietrzyk[9], U. Pietrzyk[17q)], B. Pönsgen[4], B. Povh[5], P. Renton[11], P. Ribarics[7m)], K. Rith[3c)], E. Rondio[16a)], L. Ropelewski[16a)], D. Salmon[13], A. Sandacz[16n)], M. Scheer[1], H. Schiemann[4], K.P. Schuler[18], K. Schultze[1], T-A. Shibata[5], T. Sloan[6], A. Staiano[5r)], H.E. Stier[3], J. Stock[3], M. Studt[4], G.N. Taylor[11s)], J.C. Thompson[12], J. Toth[7m)], S. Wheeler[13i)], L. Urban[7m)], T. Walcher[5t)], W.S.C. Williams[11], S.J. Wimpenny[8u)], R. Windmolders[10], W.J. Womersley[11v)].

(Submitted to Zeits. für Physik C)

ABSTRACT

Data are presented on exclusive ρ^0 and ϕ production in deep inelastic muon scattering from a target consisting mainly of nitrogen. The ratio of the total cross sections for ρ^0 and ϕ production is found to be $9:(1.6 \pm 0.4)$ at $\langle Q^2 \rangle = 7.5$ GeV^2, consistent with the SU(3) prediction of 9:2. The t dependence for exclusive ρ^0 production is found to become shallower as Q^2 increases and, for large Q^2, the t dependence is typical of that for a hard scattering process. Furthermore, the ratio of the cross sections for coherent: incoherent production from nitrogen is found to decrease rapidly with Q^2. Such behaviour indicates that even for exclusive vector meson production the virtual photon behaves predominantly as an electromagnetic probe and that the soft hadronic properties, evident in the vector dominance behaviour of real photons ($Q^2=0$), die out rapidly for large space-like values of Q^2.

For footnotes see next page.

a) University of Warsaw, Warsaw, Poland, partly supported by CPBP-01.06.
b) Permanent address: University of Bielefeld, Bielefeld, Germany.
c) Now at MPI für Kernphysik, Heidelberg, Germany.
d) Now at TESA S.A., Renens, Switzerland.
e) Now at British Telecom, Ipswich, England.
f) Now at Jet, Joint Undertaking, Abingdon, England.
g) Now at University of Manchester, England.
h) Now at RAL, Chilton, England.
i) Now at CERN, Geneva, Switzerland.
j) Permanent address: University of California, Santa Cruz, U.S.A.
k) Now at L.A.L, Université de Paris Sud, Orsay, France.
l) Now at Beiersdorf A.G., Hamburg, Germany.
m) Permanent address: Central Research Institute for Physics of the Hungarian Academy of Science, Budapest, Hungary.
n) Institute for Nuclear Studies, Warsaw, Poland, partly supported by CPBP-01.09.
o) Now at NRC, Ottawa, Canada.
p) Now at AT&T, Naperville, Illinois, U.S.A.
q) Now at MPI für Neurologische Forschung, Köln, Germany.
r) Now at INFN, Torino, Italy.
s) Now at University of Melbourne, Victoria, Australia.
t) Now at University of Mainz, Mainz, Germany.
u) Now at University of California, Riverside, CA 9252, U.S.A.
v) Now at University of Florida, Gainsville, U.S.A.

Addresses

1) III. Physikalisches Inst. A, Physikzentrum, Aachen, Germany.
2) CERN, Geneva, Switzerland.
3) Fakultät für Physik, Universität Freiburg, Germany.
4) II Institut für Experimental physik, Universität Hamburg, Germany.
5) Max-Planck Institute für Kernphysik, Heidelberg, Germany.
6) Department of Physics, University of Lancaster, England.
7) Laboratoire d'Annecy de Physique des Particules, IN2P3, Annecy-le-Vieux, France.
8) Department of Physics, University of Liverpool, England.
9) Centre de Physique des Particules, Faculté des Sciences de Luminy, Marseille, France.
10) Faculté des Sciences, Université de L'Etat à Mons, Belgium.
11) Nuclear Physics Laboratory, University of Oxford, England.
12) Rutherford-Appleton Laboratory, Chilton, Didcot, England.
13) Department of Physics, University of Sheffield, England.
14) Istituto di Fisica, Università di Torino, Italy.
15) Gustav Werners Institut, University of Uppsala, Sweden.
16) Physics Institute, University of Warsaw, and Institute for Nuclear Studies, Warsaw, Poland.
17) Fachbereich Physik, Universität Wuppertal, Germany.
18) Physics Department, Yale University, Connecticut, U.S.A.

INTRODUCTION

Exclusive lepto-production, e(or μ) N → e (or μ)VN, and photo-production ($Q^2 = 0$) (γN → VN) of vector mesons, V, has been studied previously in many different experiments [1]. These studies have been made mainly at rather low incident photon energies, ν, and four-momentum transfer squared, Q^2, (typically $\nu \lesssim 20$ GeV, $Q^2 < 3$ GeV^2). These data indicate that the photon has hadron-like properties which may be described by the vector dominance model (VDM) [1]. In real photo-production ($Q^2 = 0$) the process is observed to be mainly diffractive and the helicity of the ρ° is nearly the same as that of the incident photon in the s channel helicity frame, i.e. helicity is conserved in this frame. In contrast, a measurement performed at larger values of Q^2 ($2 < Q^2 < 20$ GeV^2) [2] using a hydrogen target showed that the ρ° mesons were produced dominantly in a helicity zero state. Comparison of the measured cross sections with those found at lower Q^2 [7] shows that the production is mainly from transversely polarised virtual photons (i.e. helicity ± 1). This indicates that, at larger values of Q^2, s-channel helicity is no longer conserved. Furthermore, as Q^2 increases the dependence of the differential cross section on the 4-momentum transfer, t, from the photon to the ρ° falls less steeply. For $Q^2 \gtrsim 5$ GeV^2 the t dependence becomes inconsistent with diffractive production mechanisms. These properties suggest that for large Q^2 exclusive vector meson production becomes a hard scattering process and it seems no longer appropriate to use the VDM to describe such processes (for $Q^2 > 2$ GeV^2). Moreover the simple propagator behaviour of the exclusive ρ° and J/ψ cross section which is well established by many experiments [1,2,7,8,9] points to a single production mechanism in the whole Q^2 range, showing up as a hard scattering process at large Q^2 and reproducing the VDM behaviour towards the photo-production regime.

In this paper, new data are presented which test further these ideas. The data were taken using μ^+ beams of 120 and 200 GeV incident energy, scattering from an ammonia target, so that most of the events occur off nitrogen nuclei. Both coherent and incoherent production of exclusive ρ^0 mesons have been studied and the total yield of exclusive ϕ mesons has been measured.

EXPERIMENTAL PROCEDURE

The experiment was performed in the M2 muon beam at the CERN SPS using the EMC forward spectrometer to detect the scattered muon and the fast forward produced hadrons. Figure 1 shows a schematic diagram of the apparatus. The spectrometer and the analysis procedures were similar to those described in [2,3,4] with the following differences. The drift chambers upstream of the magnet in the original spectrometer [4] operated in a high background environment and were subject to substantial efficiency corrections. Here they have been replaced by the multiwire proportional chambers labelled PV1 and PV2 in fig. 1, allowing data to be taken efficiently at incident muon intensities up to 4×10^7 muons per SPS pulse, which is a factor 3 higher than previously. The multiwire proportional chambers P4 and P5 (fig. 1) were also installed to cover the central regions of the drift chambers W4 and W5. The latter chambers tended to become inefficient in this region after prolonged exposure to radiation due to the deposition of silicon compounds on the sense wires. In addition, the small multiwire proportional chambers labelled POA, POD and POE in fig. 1 were installed to cover the deadened chamber areas in the beam region. The apparatus had good efficiency for charged hadrons of momenta greater than ~ 5 GeV.

The target was an 80 cm long polarised target, the main purpose of which was to study the spin dependence of the proton structure function. It consisted mainly of ammonia with a small admixture of helium (~10% by weight). The mean atomic weight of the target was

10.8. Other thinner targets, located about 1 m downstream (fig. 1) were also present during most of the data taking. Only events originating from the polarised target (summed over the different spin alignments) are used in the present analysis. The data were taken in three experimental runs, two at 200 GeV and one at 120 GeV incident muon energy, using a trigger corresponding to a scattering angle $\theta_\mu \gtrsim 0.75°$.

DATA ANALYSIS AND RESULTS

The data were passed through a chain of analysis programmes in which pattern recognition, track and vertex reconstruction were carried out. Events containing a reconstructed scattered muon which was consistent with having produced the trigger and a pair of hadrons of opposite charges were selected for further analysis. Events were rejected if the ratio of the energies deposited in the electromagnetic part of the calorimeter (H2, fig. 1) to the sum of the electromagnetic and hadronic parts was greater than 0.8 for either non-muon track. In this way, electron-positron pairs were removed from the data sample. The loss of hadron tracks due to this procedure was measured from the data by extrapolating the distribution of the measured ratios into the rejected region. The loss was found to be small (~ 6%).

In the analysis presented here, further details of which are given in [5], the standard variables employed in deep inelastic scattering were used. These are Q^2, ν and W the total energy in the virtual photon-proton centre of mass system. The data were selected with $Q^2 > 1$ GeV^2 and $y < 0.9$ where $y = \nu/E$ and E is the energy of the incident muon. For the comparison of the ρ° and ϕ yields the 200 GeV data were used and restricted to the ranges $2 < Q^2 < 25$ GeV^2, $36 < W^2 < 280$ GeV^2 and the scattered muon angle was required to be greater than 10 mrad. These cuts exclude the regions where the apparatus acceptance was small or varied rapidly or where QED radiative corrections are large.

To select exclusive events containing a single hadron pair, the total energy of the pair was required to be greater than 0.92ν. As shown in [2], there is only a small residual contamination of events containing an extra undetected hadron with these selection criteria. Figure 2 shows the invariant mass distributions of the hadrons treated as either K^+K^- or $\pi^+\pi^-$ pairs. Clear peaks are seen at the ρ° mass in the $\pi^+\pi^-$ distribution and at the ϕ mass in the K^+K^- distribution. In these distributions events falling in the ρ° mass region $(m_\rho - \Gamma_\rho/2)$ treated as $\pi^+\pi^-$ pairs were excluded from the K^+K^- spectrum. Similarly events falling in the ϕ mass region $(m_\phi-\Gamma_\phi) < m_{KK} < (m_\phi+\Gamma_\phi)$ when treated as K^+K^- pairs were excluded from the $\pi^+\pi^-$ mass spectrum. Here m_ρ, m_ϕ, Γ_ρ and Γ_ϕ are the masses and widths of the ρ° and ϕ mesons, respectively. Only a small number of events satisfied both conditions simultaneously and the correction for the loss of these events was included in the acceptance calculation.

The acceptance of the apparatus was computed by Monte Carlo simulation in which exclusive ρ° and ϕ events were generated and weighted according to parameterisations of the data in [2]. The total numbers of ρ° and ϕ mesons were determined by applying acceptance corrections to the mass distributions (fig. 2) and by fitting a p-wave Breit-Wigner distribution together with a smooth background function to each. The corrected total number of elastic ρ° and ϕ mesons were found to be 538 ± 40 and 94 ± 24, respectively, (200 GeV data). From these yields the ratio of the cross sections is

$$\frac{\sigma(\gamma^* p \to \rho^\circ p)}{\sigma(\gamma^* p \to \phi p)} = \frac{9}{1.6 \pm 0.4}$$

at a mean value of Q^2 of 7.5 GeV^2. The estimated systematic error of ~10% is much smaller than the quoted statistical error. The observed ratio is consistent with the value of 9:2 expected from SU(3) flavour symmetry. However, it is larger than the value of $9:(0.65 \pm 0.03)$ obtained from the measurement in real photon production ($Q^2 = 0$) at similar incident photon energies [6].

Figure 3(a) shows this result together with previous measurements of the ratio of the cross sections for elastic ρ° to elastic ϕ production as a function of Q^2. Figure 3(b) shows the cross sections for elastic ρ° photo-production on hydrogen [2,7] and elastic J/ψ photo-production obtained on iron [8] as a function of Q^2. It can be seen that these cross sections become almost equal at high Q^2. Figure 3(c) shows the same data presented as a ratio of the cross sections where the ratio was calculated by interpolating between the J/ψ points (fig. 3b). The smooth curves in figs. 3(a) and 3(c) show the predictions of the following simple model. Firstly, it is assumed that in the limit of large Q^2 ($Q^2 >> m_i^2$, where m_i is the mass of the vector meson i) the ratio $\sigma_\rho : \sigma_i$ approaches the value expected from flavour symmetry [1] i.e. 9:2 for ϕ and 9:8 for J/ψ. Secondly, in the intermediate Q^2 range it is assumed that the cross section follows the form $1/(m_i^2 + Q^2)^2$, a behaviour which is well established for the Q^2 dependence of the ρ° and J/ψ cross sections [1,2,7,8,9]. With these assumptions the ratio of the cross sections will vary as

$$R = \frac{\sigma_i}{\sigma_\rho} = \frac{c_i}{9} \frac{(m_\rho^2+Q^2)^2}{(m_i^2+Q^2)^2}$$

with $c_i = 2$ for ϕ and 8 for J/ψ. Both curves without free parameters give a reasonable representation of the data in figs. 3a) and c). This indicates that the production mechanisms for the elastic vector mesons ρ°, ϕ, and J/ψ are similar in the whole Q^2 range with the differences in the production cross-sections being determined by the different meson masses which are related to the quark masses.

A theoretical model for the process has been developed by Donnachie and Landshoff [16]. This diffractive model, involving Pomeron exchange, would imply s channel helicity conservation contrary to the observations in [2]. It also predicts steeper slopes for the t distribution than observed at the highest values of Q^2 (see below).

Figure 4 shows the yields for elastic ρ° production as function of $t' = |t-t_{min}|$, where t is the four-momentum transfer squared between the virtual photon and the ρ° meson and t_{min} is the kinematic minimum value. The acceptance of the apparatus as a function of t' is essentially flat so that no correction is necessary. The peaks at small values of t' correspond to coherent production from the nitrogen in the target, smeared by experimental resolution. The lines show fits of the form $e^{-bt'}$ to the data for $t' > 0.2$ GeV^2, which excludes the coherent region. The slopes of the fitted lines decrease as Q^2 increases, indicating a transition from a soft to a hard scattering process. This is consistent with the behaviour described in [2] and the measured values of the slopes at each Q^2 show reasonable agreement within the errors with the hydrogen data as shown in fig. 5. The observed shallow t slopes at the largest values of Q^2 are ascribed in [16] to the residual inelastic background. However, even if the assumption is made that this background is flat in t, the combination of such a background with the predicted t distribution of [16] fails to represent the shape of the data at the largest value of Q^2 in fig. 4. This implies that the explanation offered in [16] of the shallow t slopes at large Q^2 fails to reproduce the observations.

The polarisation of the ρ° in the s-channel helicity frame was investigated by measuring the density matrix element r^{04}_{00} from the decay angular distribution in the ρ° rest frame [2]. This density matrix element can be identified with the probability to produce a ρ° in a helicity zero state. The mean value of the density matrix element $\langle r^{04}_{00} \rangle$ was found to be 0.72 ± 0.08 for $t' > 0.2$ GeV^2 at $\langle Q^2 \rangle = 7.5$ GeV^2. This is consistent with the measurement on hydrogen in [2] and shows that the angular distribution varies almost as $\cos^2\theta$ in the s-channel frame. For $t' < 0.2$ the angular distribution is approximately flat showing that it is a mixture of $\sin^2\theta$ and $\cos^2\theta$ dependences. This suggests that, for $t' < 0.2$, the cross section is a mixture of coherent (diffractive) and incoherent parts where in the latter part the ρ° spin flips as indicated by the data at higher t'.

The straight line fits in fig. 4 were extrapolated under the coherent peak in order to estimate the ratio of the coherent (σ_{coh}) to incoherent cross sections (σ_{inc}), correcting for the effects of quasi-elastic suppression in the coherent region of t' using the calculations of [17]. Figure 6 shows the ratio of $\sigma_{coh}/\sigma_{inc}$ for elastic ρ° production from nitrogen as a function of Q^2. The points at $Q^2 = 0$ were obtained by performing similar extrapolations using the data from carbon and copper targets [12,13]. The $Q^2 = 0$ point was chosen to be 2.0 from the data of McClellan et al. [12] on copper. This value comes close to an optical model calculation [15]. However, the data of Asbury et al. [13] on carbon indicate a value which is a factor 2 higher than this.

The smooth curve in fig. 6 shows the expected kinematic effect due to the increase of $t_{min} \simeq [(Q^2+m_\rho^2)/2\nu]^2$ for the 200 GeV data. To compute this curve the coherent differential cross section was assumed to decrease as e^{-50t}, as expected from the radius of the nitrogen nucleus. The data fall much faster with Q^2 than expected from such kinematic effects.

The decrease of the coherent part of the cross section with Q^2 may be understood as follows. Combining the data in [2] with those reported in [7] indicates that ρ° mesons are produced dominantly in a helicity 0 state from mainly transverse photons. In the forward direction the spin flip of the ρ° implies that the proton spin flips to conserve angular momentum. Such spin flip amplitudes will not contribute to coherent production as the nuclear state must change. Hence the coherent cross section will decrease since the relative spin flip to non-spin flip amplitudes seem to increase with Q^2 [2].

CONCLUSIONS

Exclusive ρ° and ϕ meson production has been measured in deep inelastic muon scattering from nitrogen. The ratio of the cross section for elastic ρ° and ϕ production at $\langle Q^2 \rangle = 7.5$ GeV^2 is found

to be 9:(1.6 ± 0.4). This result is close to the SU(3) prediction of 9:2. An analogous behaviour is seen in the comparison of our earlier ρ^0 and J/ψ data. The t dependence of ρ^0 production rapidly becomes harder as Q^2 increases and the coherent production from a nuclear target decreases strongly with increasing Q^2. These observations indicate that even in elastic vector meson production the virtual photon acts predominantly as an electromagnetic probe. The simple propagator behaviour of the cross section points to a single production mechanism in the whole Q^2 range, showing up as a hard scattering process at large Q^2 and reproducing the VDM behaviour towards the photoproduction region.

REFERENCES

[1] For a review see, T. Bauer, R.D. Spital, D.R. Yennie, F.M. Pipkin, Rev. Mod. Phys. 50 vol. 2 (1978) 261.

[2] EMC, J.J. Aubert et al., Phys. Lett. 161B (1985) 203.

[3] EMC, J.J. Aubert et al., Nucl. Phys. B259 (1985) 189.

[4] EMC, O.C. Allkofer et al., Nucl. Inst. and Meth. 179 (1981) 445.

[5] K. Mönig, Diplom thesis, University of Wuppertal, WuD 86-10 (1986).

[6] R.M. Egloff et al., Phys. Rev. Lett. 43 10 (1979) 657. For the evaluation of the ϕ/ρ ratio only the data in the energy range of the data presented here have been used and furthermore the ratio corrected for the revised $\phi \rightarrow K^+K^-$ branching ratio.

[7] CHIO, W.D. Shambroom et al., Phys. Rev. D26 (1982) 1.

[8] EMC, J.J. Aubert et al., Nucl. Pys. B213 (1983) 1.

[9] BFP, A.R. Clark et al., Phys. Rev. Lett. 45 (1980) 2092.

[10] E.L. Berger and D. Jones, Phys. Rev. D23 (1981) 1521.

[11] R. Baier and R. Rückl, Nucl. Phys. B218 (1983) 289.

[12] G. McClellan et al., Phys. Rev. Lett. 22 (1969) 377.

[13] J.G. Asbury et al., Phys. Rev. Lett. 19 (1967) 865.

[14] D. Aston et al., Nucl. Phys. B209 (1982) 56.

[15] For this calculation a simple spherical nucleus was assumed to perform the optical model integral. This is given in D.W.G.S. Leith; Electromagnetic Interactions of Hadrons, eds. A. Donnachie and G. Shaw, page 419.

[16] A. Donnachie and P.V. Landshoff, Phys. Lett. 185B (1987) 403.

[17] J. Bailey et al., Nucl. Phys. B151 (1979) 367.

FIGURE CAPTIONS

1. The apparatus. Key; H = scintillator trigger hodoscope, V = veto hodoscope, BH = beam hodoscope, P = multiwire proportional chamber, W = drift chamber, FSM = forward spectrometer magnet C_2 = Cerenkov counter, H_2 = calorimeter.

2. Invariant mass spectra of oppositely charged pairs of hadrons of total energy larger than 0.92 ν, treated as a) $K^{\pm}$ pairs b) $\pi^{\pm}$ pairs.

3. a) The ratio $9\sigma_{\phi}/2\sigma_{\rho}$ as a function of Q^2, including data from references [6] and [7].
   b) The photoproduction cross sections for ρ° [2,7] and J/ψ [8] as a function of Q^2. The J/ψ data is from table 1 of [8] averaged over the ν range 120-180 GeV.
   c) The ratio $9\sigma_{J/\psi}/8\sigma_{\rho}$, from the data in fig. 3b), as a function of Q^2. The smooth curves in figs. 3a) and 3c) are the predictions of the simple model described in the text.

4. The event yields as a function of $t'=|t-t_{min}|$ in different Q^2 intervals at each incident muon energy. The lines are are the fits for $t'>0.2$ GeV^2.

5. The slopes of the linear fits ($t'>0.2$ GeV^2) shown in fig. 4 as a function of Q^2, together with the data from [2] and [7] and the point at $Q^2=0$ from [14].

6. The ratio of the total coherent to incoherent cross sections as a function of Q^2. The points at $Q^2=0$ come from [12,13]. The smooth curve shows the expected decrease in this ratio from the increase of t_{min} with Q^2.

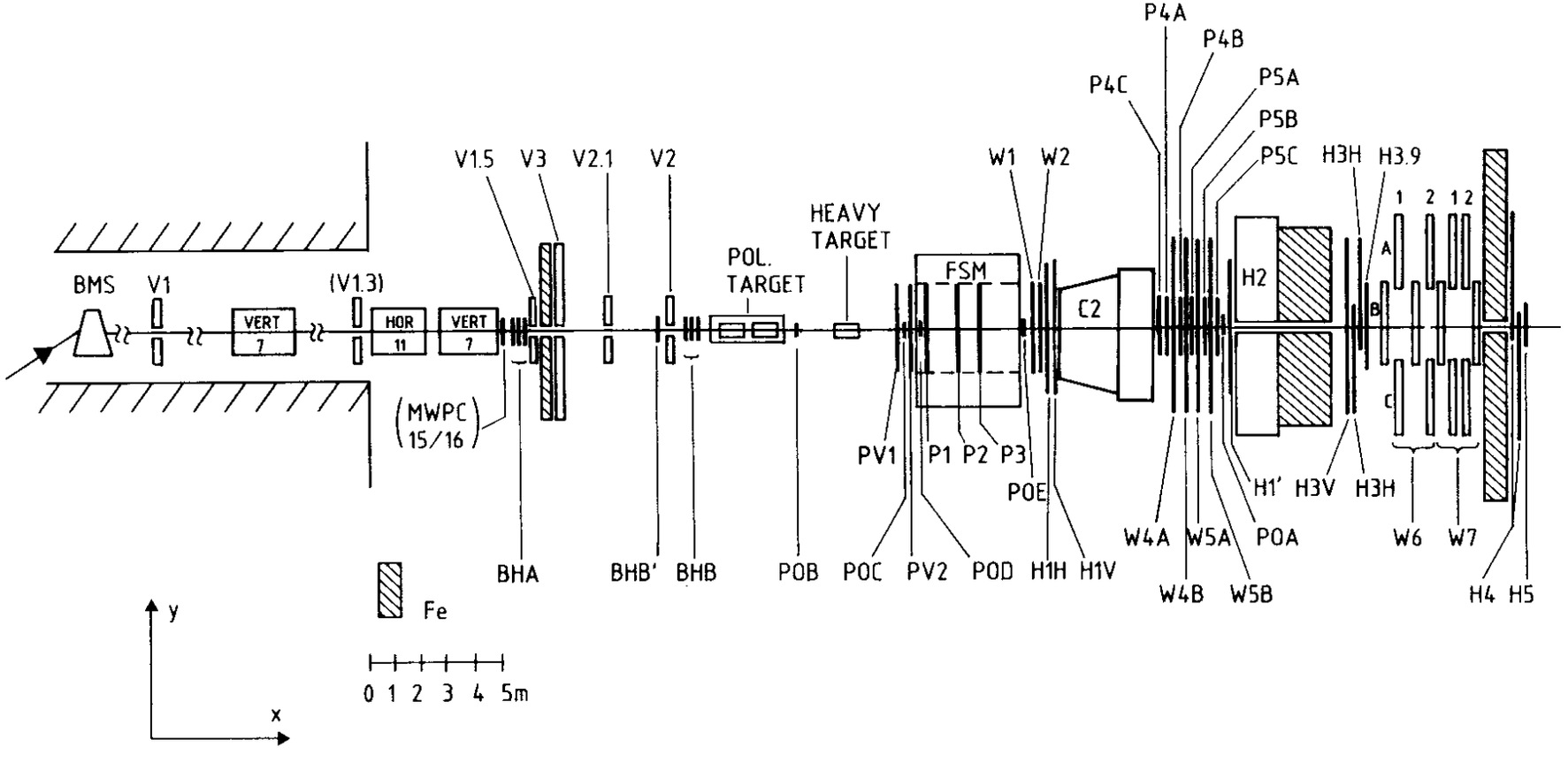
BMS
V1
(V1.3)
VERT
7
HOR
11
VERT
7
MWPC
15/16
V1.5
V3
V2.1
V2
POL.
TARGET
HEAVY
TARGET
FSM
W1
W2
C2
P4A
P4B
P4C
P5A
P5B
P5C
H2
H3H
H3.9
A
B
C
1
2
1 2
PV1
P1
P2
P3
POE
H1'
H3V
H3H
W4A
W5A
POA
W6
W7
W4B
W5B
H4
H5
BHA
BHB'
BHB
POB
POC
PV2
POD
H1H
H1V
Fe
y
x
0 1 2 3 4 5m

Fig.1

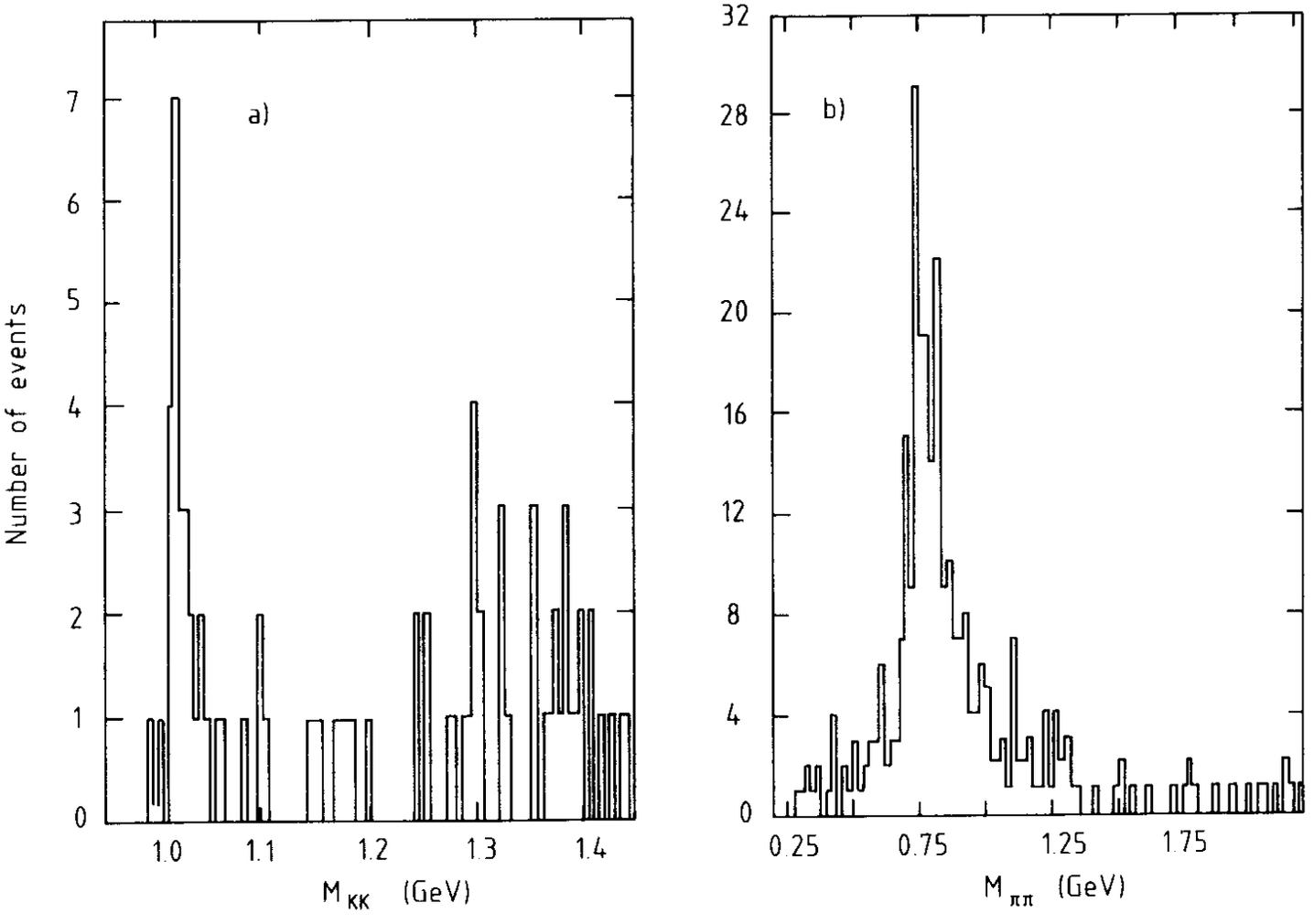
a)
b)
Number of events
0
1
2
3
4
5
6
7
0
4
8
12
16
20
24
28
32
1.0
1.1
1.2
1.3
1.4
0.25
0.75
1.25
1.75
M KK (GeV)
M ππ (GeV)

Fig.2

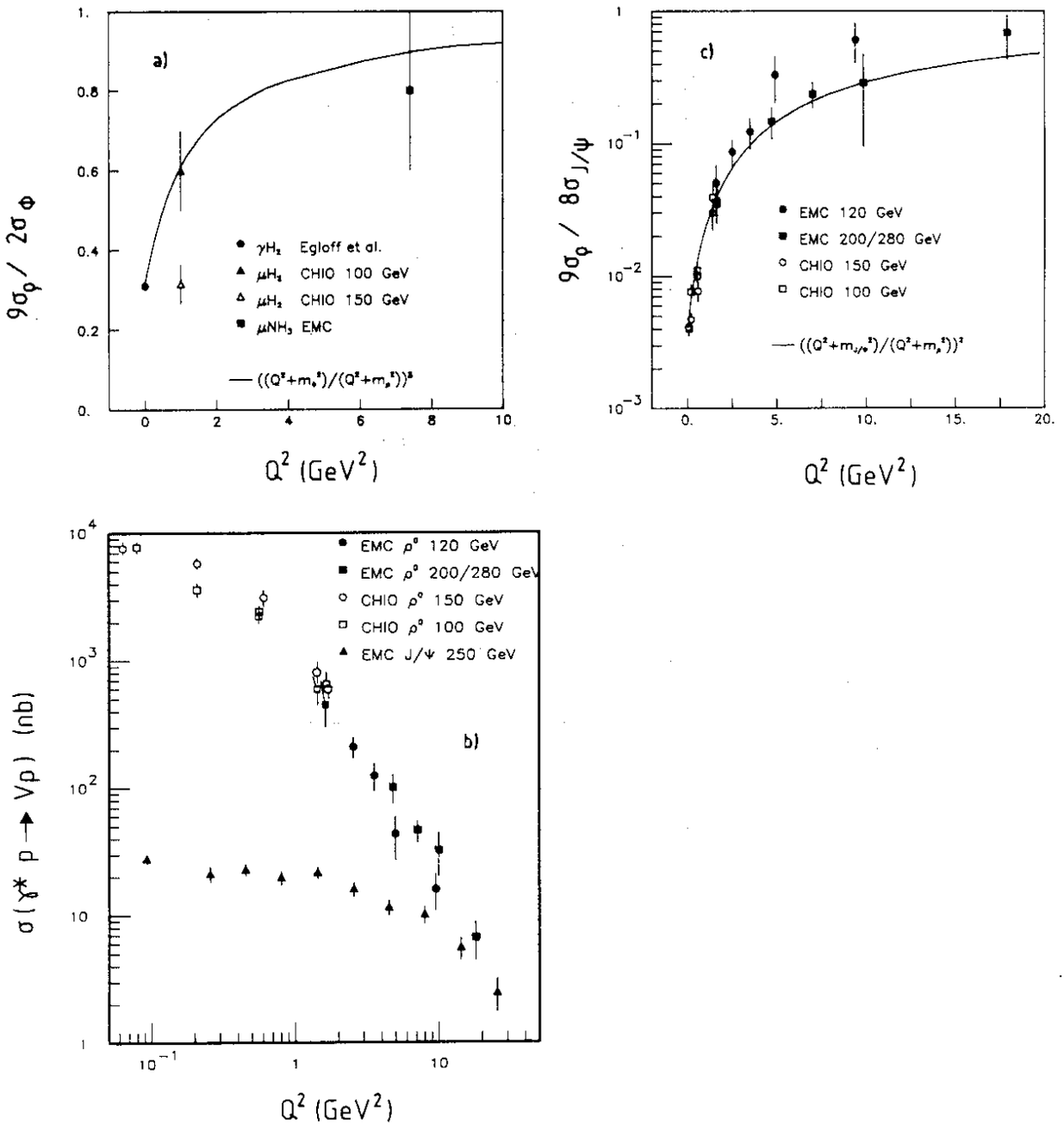
a)
$9\sigma_\rho / 2\sigma_\Phi$
γH_2 Egloff et al.
μH_2 CHIO 100 GeV
μH_2 CHIO 150 GeV
μNH_3 EMC
$((Q^2+m_\Phi^2)/(Q^2+m_\rho^2))^2$
Q^2 (GeV^2)
c)
$9\sigma_\rho / 8\sigma_{J/\psi}$
EMC 120 GeV
EMC 200/280 GeV
CHIO 150 GeV
CHIO 100 GeV
$((Q^2+m_{J/\psi}^2)/(Q^2+m_\rho^2))^2$
Q^2 (GeV^2)
b)
$\sigma(\gamma^* p \rightarrow Vp)$ (nb)
EMC ρ^0 120 GeV
EMC ρ^0 200/280 GeV
CHIO ρ^0 150 GeV
CHIO ρ^0 100 GeV
EMC J/Ψ 250 GeV
Q^2 (GeV^2)

Fig. 3

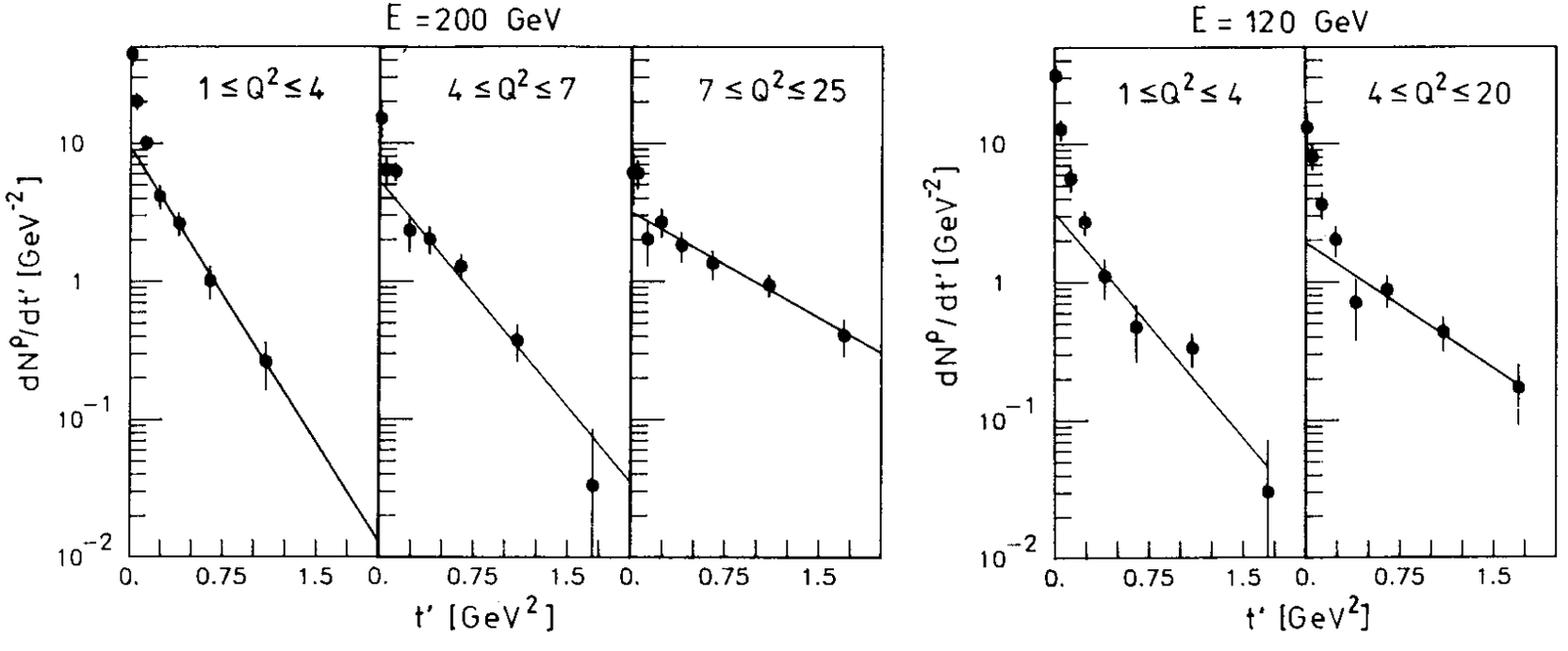
E =200 GeV
1 ≤ Q² ≤ 4
4 ≤ Q² ≤ 7
7 ≤ Q² ≤ 25
dN^ρ/dt' [GeV^-2]
10
1
10^-1
10^-2
0.
0.75
1.5
t' [GeV²]
E = 120 GeV
1 ≤ Q² ≤ 4
4 ≤ Q² ≤ 20

Fig.4

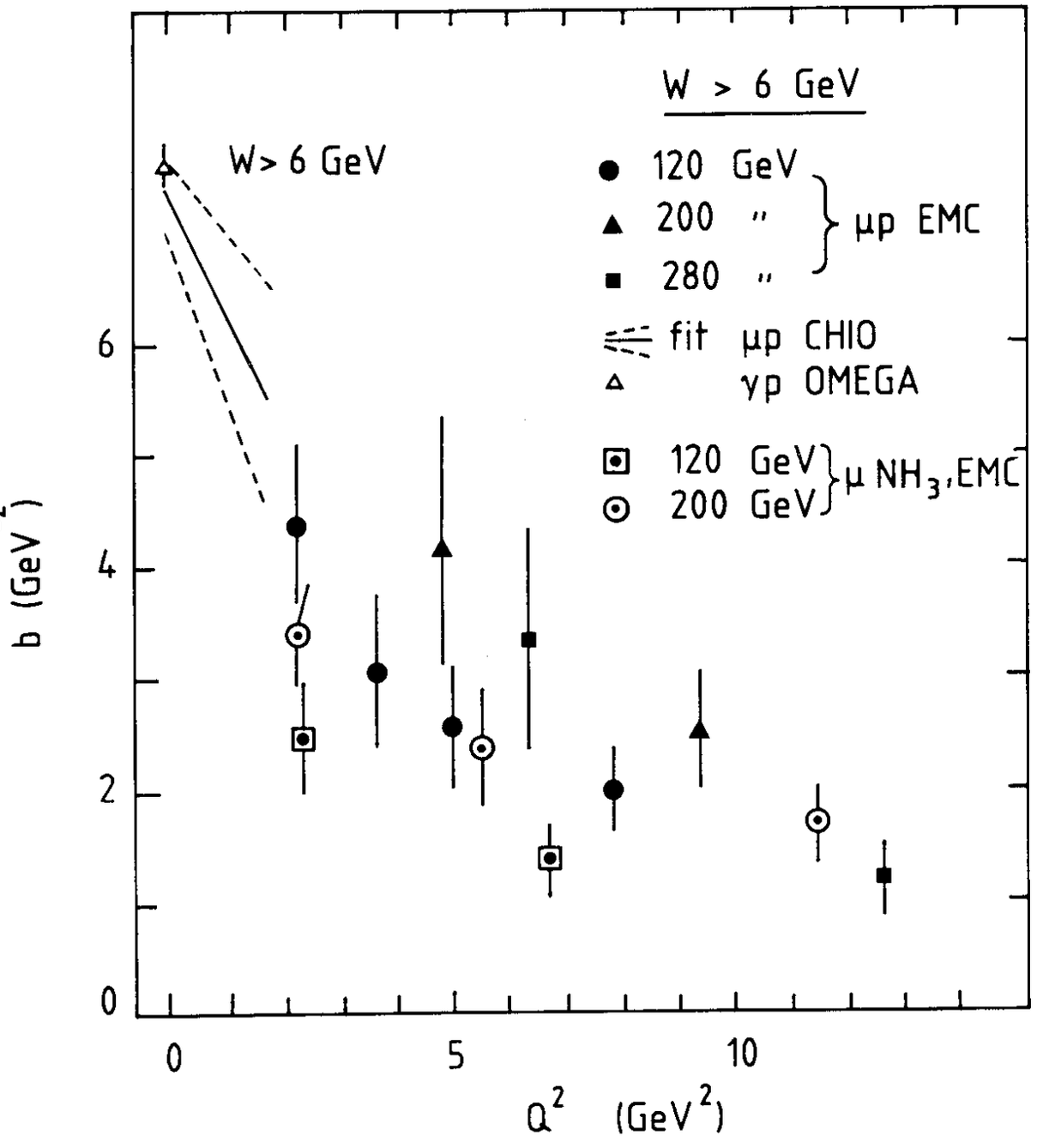
W > 6 GeV
W> 6 GeV
120 GeV
200 "
280 "
μp EMC
fit μp CHIO
γp OMEGA
120 GeV
200 GeV
μ NH3,EMC
b (GeV-2)
Q2 (GeV2)
0
2
4
6
0
5
10

Fig.5

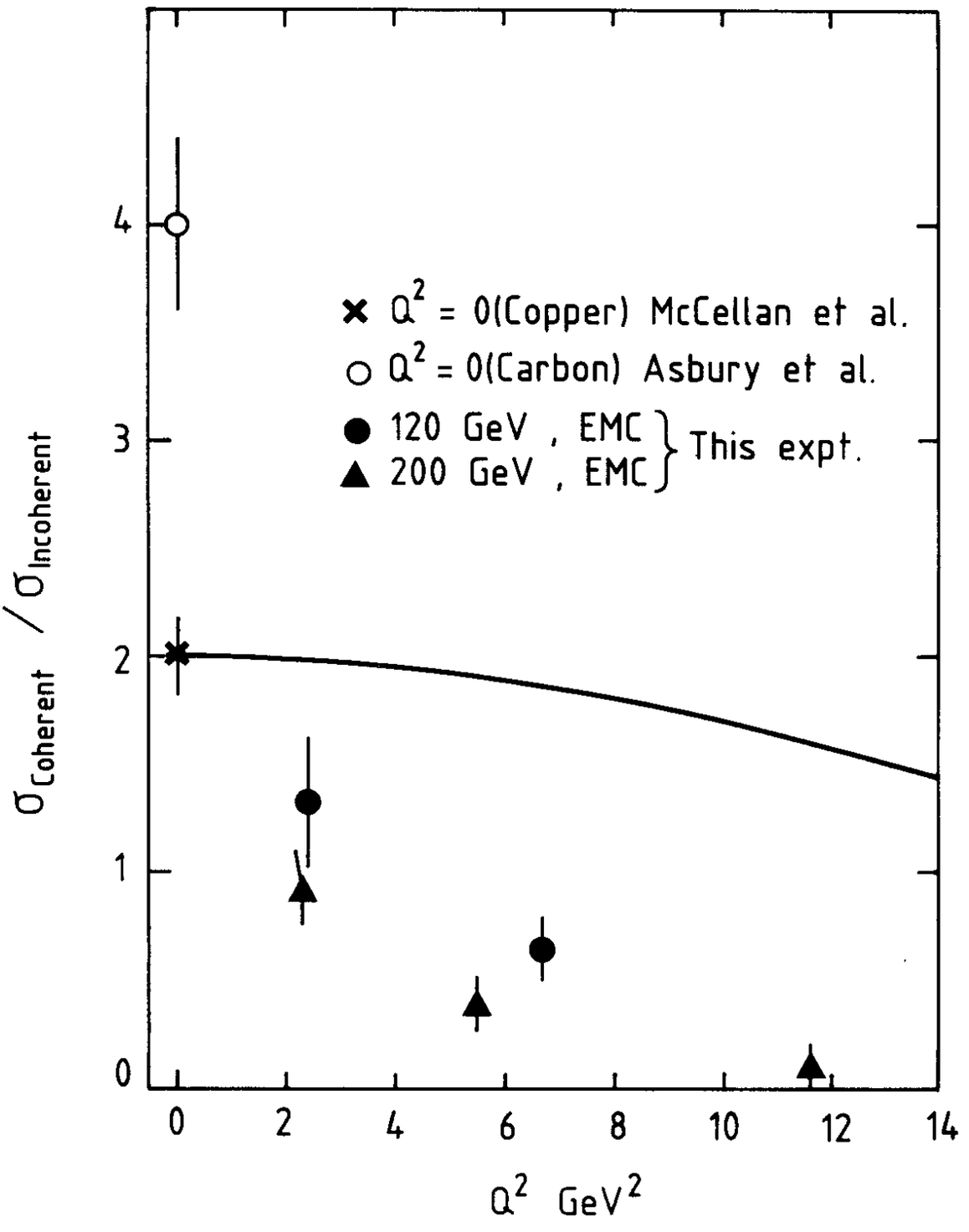
$\sigma_{Coherent} / \sigma_{Incoherent}$
4
3
2
1
0
0
2
4
6
8
10
12
14
Q^2 GeV^2
× Q^2 = 0(Copper) McCellan et al.
○ Q^2 = 0(Carbon) Asbury et al.
● 120 GeV , EMC
▲ 200 GeV , EMC
} This expt.

Fig.6